Chitin and chitosan – structurally-related precursors of dissimilar hard carbons for Na-ion battery

J. Conder, C. Vaulot, C. Marino, C. Villevieille, Camelia Ghimbeu

Chitin and Chitosan – Structurally-related Precursors of Dissimilar Hard Carbons for Na-ion Battery

*Joanna Conder[1,2], Cyril Vaulot[1,2], Cyril Marino[3], Claire Villevieille[3], Camélia Matei Ghimbeu[1,2,4]**

[1]Université de Haute-Alsace, Institut de Science des Matériaux de Mulhouse (IS2M), CNRS UMR 7361 F-68100 Mulhouse, France

[2]Université de Strasbourg, F-67081 Strasbourg, France

[3]Paul Scherrer Institute, Electrochemistry Laboratory, CH-5232 Villigen PSI, Switzerland

[4]Réseau sur le Stockage Electrochimique de l'Energie (RS2E), FR CNRS 3459, 80039 Amiens Cedex, France

*Corresponding author : camelia.ghimbeu@uha.fr

ABSTRACT

Hard carbons (HCs) prepared from renewable precursors are promising cost-effective electrode-material candidates for the application in Na-ion battery. Usually these materials are derived from cellulose. Here, however, we demonstrate that other polysaccharides, such as chitin and chitosan, can be as well up-and-coming parent materials of HCs. Despite structural similarities, thermal decomposition of these two biopolymers proceeds differently, contributing to the discrepancies in physicochemical properties of resulting HCs. Although chitin- and chitosan-derived HCs have comparable d-spacings and crystallite sizes, solid state pyrolysis of the former biopolymer leads to micro-mesoporous material with significant specific surface area, while that of chitosan yields non-porous carbon. Despite that, both materials deliver similar initial specific charge of 280 mAh g^{-1} (at C/10 rate) and their electrochemical performance starts to diverge only upon longer cycling at higher rate. With time, inorganic contaminants present in chitosan-derived HC presumably delay the diffusion of Na-ions to and within the electrode, and slow down the rate of electrochemical reactions, eventually triggering polarization build-up. Further optimization of the chitosan-derived HC through acid-treatment enables unblocking some of the micropores and increasing the carbon content in this material, therefore enhancing its active surface area and suppressing continuous fading of the specific charge.

KEYWORDS: hard carbon, chitin, chitosan, Na-ion battery, biomass

1. INTRODUCTION

Antibacterial, biodegradable, easy to functionalize and modify, naturally abundant, and nontoxic[1, 2] – the list of chitin and chitosan properties is almost endless as is the number of applications for which these two linear polysaccharides are being extensively explored and in which they are already implemented. They serve as efficient drug delivery systems, coagulants and sludge dewatering aid,[1] and finishing agents for textiles with specific properties[3] (mosquito- and water-repellent fabrics).[4] In addition, chitosan, the N-deacetylated form of chitin known for its hemostasis-stimulating properties,[5] is tested in combination with a silk protein for the preparation of implantable films and scaffolds for surgical closure and wound healing.[2, 6] In the latter case, chitosan-laden bandages have already proved invaluable in hastening blood clotting in fresh wounds of US soldiers.[7] These results encouraged researchers to test the healing properties of this shrimp-shell derived biopolymer in conditions even more conductive to bacteria growth, namely in space. Contrary to chitosan, chitin did not "conquer the space", mainly because of its very low, if any, solubility in common organic solvents. Instead, it was investigated in more "earthbound" applications, often related to energy storage. In supercapacitors, for example, chitin was studied as an alternative to "standard" polytetrafluoroethylene (PTFE) binder.[8] The use of this linear polysaccharide naturally doped with nitrogen in place of PTFE significantly enhanced the affinity of the electrolyte to the electrode surface, thereby shortening its wetting time. It also improved the charge propagation at the electrode/electrolyte interface and, thus, the reversibility of the charge – discharge processes. Despite that, the use of chitin as binder for supercapacitor electrodes did not attract great attention at industrial scale and the fault of this lay again in its scarce solubility in organic solvents. Recently, the interest in chitin for energy-storage

applications has shifted towards the preparation of nitrogen-doped (porous) carbons, e.g. porous carbon fibers[9] and nanofibrous microspheres with hierarchical porosity.[10] This is because the presence of nitrogen in carbon network alters the wettability and polarity of its surface, as well as its electronic properties, and, thus, may trigger Faradaic redox reactions with electrolyte ions. The latter, especially important for electrochemical capacitors (supercapacitors), largely depends on the amount of the dopant and its bonding with carbon atoms.[9] Because high temperature favors the decomposition of acetamido groups in chitin chains, direct pyrolysis of this polysaccharide often results in carbon hardly doped with nitrogen. Attempts to overcome this issue include, among others, stabilizing nitrogen in carbon at low temperature through hydrothermal carbonization prior to its further processing.[11] The struggle to preserve nitrogen in carbon structure after pyrolysis also concerns chitosan. Perhaps this is the reason why this deacetylated form of chitin was so far mostly tested as a binder[12, 13] and less often as a main electrode component, the active material.[14] This trend may, however, start to change given the recent (re-)emergence of non-lithium battery chemistries and growing interest in asymmetric and hybrid supercapacitors. As carbohydrate polymers, chitin and chitosan are predisposed to convert into non-graphitizable or hard carbons upon thermal treatment and, thus, to be successfully implemented as negative-electrode materials in Na-ion battery. Therein, they are expected to deliver a specific charge comparable to HCs derived from cellulose (> 300 mAh g^{-1}), their structural analogue. Unfortunately, very low carbon yield (C-yield) of the heat-treated cellulose (less than 20%) and the necessity of controlling dehydration and cross-linking degree continue to outweigh the use of the HC derived from this sustainable polymer as negative electrode material for Na-ion batteries.[15] Besides cellulose, glucose,[16] lignin,[17] pitch-lignin mixture,[18] phenolic resin,[19] pitch-phenolic resin mixture,[20] and other organic polymers and biomass are often used as

HC parent materials. Among them, HCs derived from lignin, phenolic resins, and their mixture with pitch come to the fore owing to significantly higher C-yield than that of cellulose-derived HC (> 40%) and decent electrochemical performance.[18] Depending on the source of the organic polymer / biomass, its preparation, and pyrolysis conditions, average reversible specific charge of the Na-ion cells assembled with HCs obtained from these cellulose-competitors is between 250 and 370 mAh g^{-1}, while first-cycle Coulombic efficiency typically reaches 70–80%.[21] Unfortunately, lignin-derived HCs are usually plagued with difficult-to-remove inorganic impurities strongly affecting their performance, whereas high toxicity of phenolic resins does not render them seeking-for HC precursors, unless these formaldehyde derivatives are prepared via "green" synthetic routes.[22]

Here, we present a study of both biopolymers, chitin and chitosan, as precursors of hard carbons (HC) for Na-ion battery. We attempt to correlate the electrochemical performance of the obtained HCs with the morphology, structure, surface chemistry, and texture of these materials, often missing in the literature. We search not only for a cause of low first-cycle Coulombic efficiency and fading specific charge but also for a cure for undesired HC characteristics, such as the presence of inorganic impurities.

2. EXPERIMENTAL

2.1 Biopolymers characterization. Elemental composition of chitin (chitin from shrimp shells, Sigma-Aldrich, a polymer of acetyl glucosamine of varying lengths) and chitosan (Sigma-Aldrich, M_w between 190'000 and 310'000 Da) was determined by means of Thermo Electron Flash EA 1112 analyzer. Thermal decomposition of these two biopolymers was studied by thermogravimetric analysis (TGA) and temperature-programmed desorption coupled to mass

spectroscopy (TPD-MS). In the former analysis, both carbon precursors were heated from 30 to 900°C at a heating rate of 5°C min^{-1} under the flow of nitrogen and the weight loss was continuously monitored by METTLER-TOLEDO TGA 851e. Similar temperature range was used during the heat treatment of chitin and chitosan in the latter analysis, TPD-MS, which was performed under vacuum at a slower heating rate of 1°C min^{-1} to avoid saturation of the MS detector. Prior to the analysis the samples were outgassed overnight under dynamic vacuum at room temperature. The concentration of the gases desorbing from the surface of the chitin and chitosan was monitored as a function of temperature and analyzed with the mass spectrometer calibrated to N_2, H_2, CO, CO_2, and H_2O.

2.2 Preparation and modification of hard carbon. A series of hard carbons (HCs) was prepared from either chitin or chitosan by heating up to 1300°C (dwell time of 2h) (Figure 1). The thermal treatment was performed under argon at a moderate heating rate of 5°C min^{-1}. The annealing temperature was chosen based on the previous studies from our group[23], as a good compromise between the concentration of defects, the d-spacing, and the porosity. The obtained carbons, chitin- and chitosan-derived HC, thereafter denoted as HC-cht-1300 and HC-chs-1300, respectively, were subsequently characterized by multiple surface and bulk techniques.

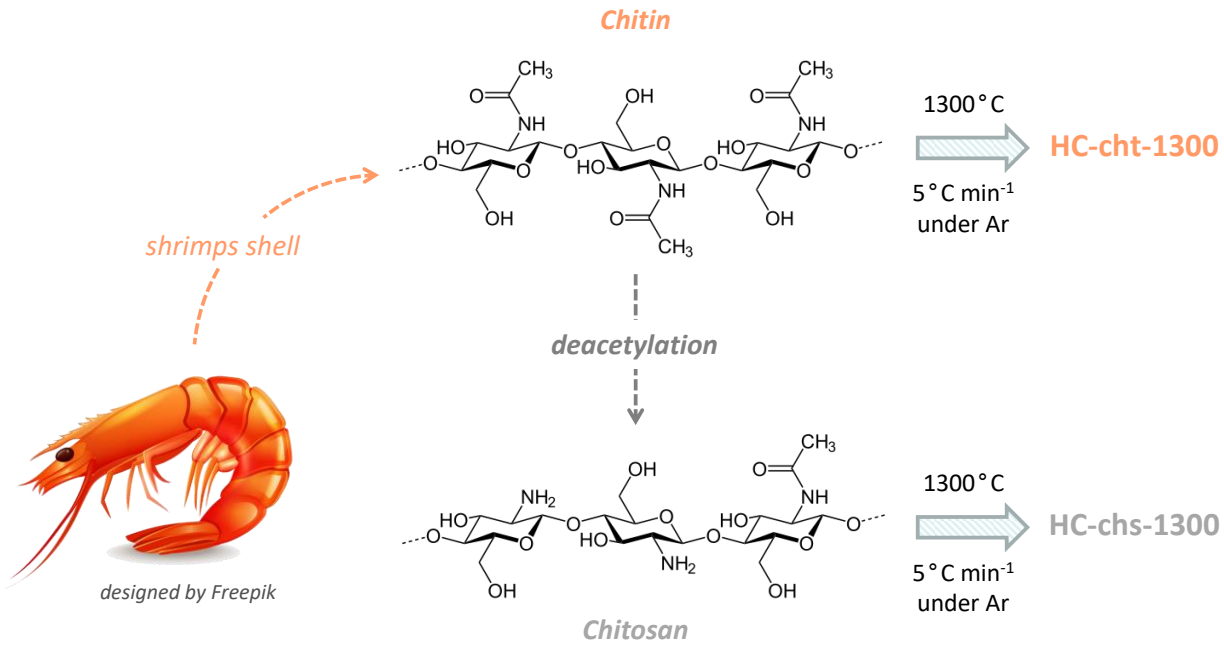

Figure 1 Schematics illustrating preparation of hard carbons from chitin and chitosan. The shrimp graphics was designed by Freepik.[24]

To study the impact of the impurities, mainly Ca and some alkali metals inherited from the parent material, on the structure and properties of the chitosan-derived carbon one batch of HC-chs-1300 was washed with 20% hydrochloric acid (HCl_{aq}) solution in water. It was subsequently neutralized with sequential water washes to remove residual chloride species from carbon pores,[25] and dried for few hours at 80°C to reduce the content of moisture. The properties of the acid-treated HC-chs-1300 were also systematically examined by multiple characterization techniques described in the next section.

2.3 Physicochemical characterization. The pore structure of the HCs was investigated by gas adsorption. N_2 and CO_2 were both used as adsorbing gas molecules to probe the meso- and

microporosity of these materials. The isotherms were measured with ASAP 2420 and 2020 porosity analyzers (Micrometrics) at 77 and 273 K, respectively, on previously outgassed samples (300°C, overnight, under primary vacuum). Specific surface area, SBET, was calculated based on the data acquired in the low relative pressure (P/P_0) range between 0.05 and 0.3. Total pore volume, V_t, was estimated from the amount of N_2 adsorbed at P/P_0 of 0.99, whereas micropore and ultra-micropore volumes were determined using the Dubinin-Radushkevich equation. Finally, the meso- and micropore size distributions were obtained from the adsorption branch of the N_2 and CO_2 isotherms, respectively, using NLDFT standard slit models implemented in a SAIEUS software supplied by Micrometrics.[26] The volume ratio (in %) of closed, R_{CP}, and open pores, R_{OP}, was estimated from the following equations:

$$R_{CP}(\%) = \left(\left(\frac{1}{d_{He}} - \frac{1}{2.32}\right) / \left(V_{OP} + \frac{1}{d_{He}}\right)\right) \cdot 100 \quad (1)$$

$$R_{OP}(\%) = \left(V_{OP} / \left(V_{OP} + \frac{1}{d_{He}}\right)\right) \cdot 100 \quad (2)$$

by taking into account apparent density of graphite (2.32 g cm^{-3}) and respective HC (measured by means of helium pycnometer; detailed experimental protocol can be found in Supporting Information), and V_t obtained from N_2 adsorption measurements.[27]

All HCs were characterized structurally by X-ray diffraction (XRD). The diffraction patterns were collected with a D8 ADVANCE A25 powder diffractometer (Bruker) in Bragg-Bretano reflection geometry using Cu $K\alpha_{1,2}$ radiation. The crystallite size, L_c, was calculated from (002) graphite peak according to the Scherrer equation:

$$L_c = \frac{0.9\lambda}{\beta \cos\Theta} \quad (3)$$

where λ is the X-ray wavelength, β is the full-width at half-maximum corrected for instrument broadening, and θ is the Bragg angle.[28-30] The morphology of the HCs was examined by scanning

and transmission electron microscopies (SEM, TEM). SEM analysis was performed at 10 kV with Ultra 55, Carl Zeiss instrument and coupled to energy dispersive X-ray spectroscopy (EDX, EDAX TSL, AMETEK, Ultra 55, Carl Zeiss). TEM images were recorded using a JEOL ARM-200F instrument operated at 200 kV.

Chemical analysis of the extreme surface of HCs (first 10 nm) was carried out by means of X-ray photoelectron spectroscopy (XPS, VG SCIENTA Model SES-2002 Spectrometer). Bulk surface chemistry of chitin- and chitosan-derived HCs was studied by TPD-MS using a measurement protocol similar to that described previously for their respective precursors (Section 2.1, heating up to 950°C under vacuum). The only difference was the heating rate, which in the case of the HCs was set to 5°C min^{-1}. Having removed the oxygen-containing groups from the surface of the HC, it was possible to calculate the number of active sites. For this purpose, after the TPD, the "clean" HC was heated up to 300°C at which it was exposed to O_2 for 10 h. The remaining non-chemisorbed O_2 was removed from the system and the HC was heated again to 950°C (10°C min^{-1} under vacuum) to recover its surface. The amount of the desorbed CO and CO_2 was converted to equivalent oxygen concentration and used to calculate the active surface area (ASA). The latter was determined assuming that the chemisorption takes place only on the prismatic planes (edge carbons) and the formation of the C–O complex involves only one atom of oxygen and only one atom of carbon.[31, 32]

2.4 Electrode formulation. HC derived from chitin and chitosan were formulated into electrodes with carbon black (superC, Imerys) and polyvinylidene fluoride (PVDF, HSV-900, Arkema) binder suspended in N-methyl-2-pyrrolidone (NMP, Alfa Aesar), in a weight ratio of 80:10:10, respectively. Slurries were mixed using a turbo stirrer and subsequently doctor-bladed onto aluminum foil. After 12 h of vacuum-drying at 80°C, the doctor-bladed sheets were calendared to

a thickness of 100 μm. The electrodes were punched out and dried overnight under dynamic vacuum (at 80°C) prior to the insertion into an Ar-filled glovebox. On average, the loading of the HC-based electrodes was in the range of 4.5 to 6.0 mg.

2.5 Cell assembly and electrochemical characterization. HC-based electrodes were assembled into coin-type cells with sodium metal and glass fiber separator (1 mm, EUJ116, Hollingsworth & Vose) soaked with 250 μl of commercial electrolyte, 1 M sodium hexafluorophosphate ($NaPF_6$) in 1:1 v/v% mixture of ethylene carbonate (EC) and diethyl carbonate (DEC) (Kishida Chemical, battery grade). The Na-foil was prepared as described previously[33] by a simple two-step procedure comprising of removal of the native oxide layer from the surface of Na followed by its calendaring.

The Na-ion half-cells were first galvanostatically discharged to 5 mV vs. Na^+/Na and subsequently charged to 1.1 V vs. Na^+/Na at a C/10 rate for two cycles. Thereafter, the current was increased leading to a rate of C/5. Each half cycle (charge or discharge) was followed by 1 h potentiostatic step. From this point onwards, all the potentials are expressed with reference to Na metal (vs. Na^+/Na).

3. RESULTS AND DISCUSSION

3.1 From chitin and chitosan to hard carbons

Just like "the apple does not fall far from the tree", the HC does not fall far from its precursor, meaning that the chemistry and the physicochemical properties of this kind of materials are always a consequence of the selection of a parent material, its annealing conditions, and post-processing, if the latter is applied. Moreover, even if the HC-precursors are structurally related (e.g. belong to the same family of polymers) and their elemental composition is almost identical,

they do not necessary convert into similar carbons during the thermal treatment as we demonstrate herein.

At first glance it seems that both biopolymers, chitin and chitosan, undergo similar thermal decomposition with few percent mass loss between 30 and 100°C due to the evaporation of the physisorbed water followed by a major mass loss between 200 to 400°C caused by decomposition, depolymerization (Figure 2a and b), and formation of char (with an average yield of 25%).

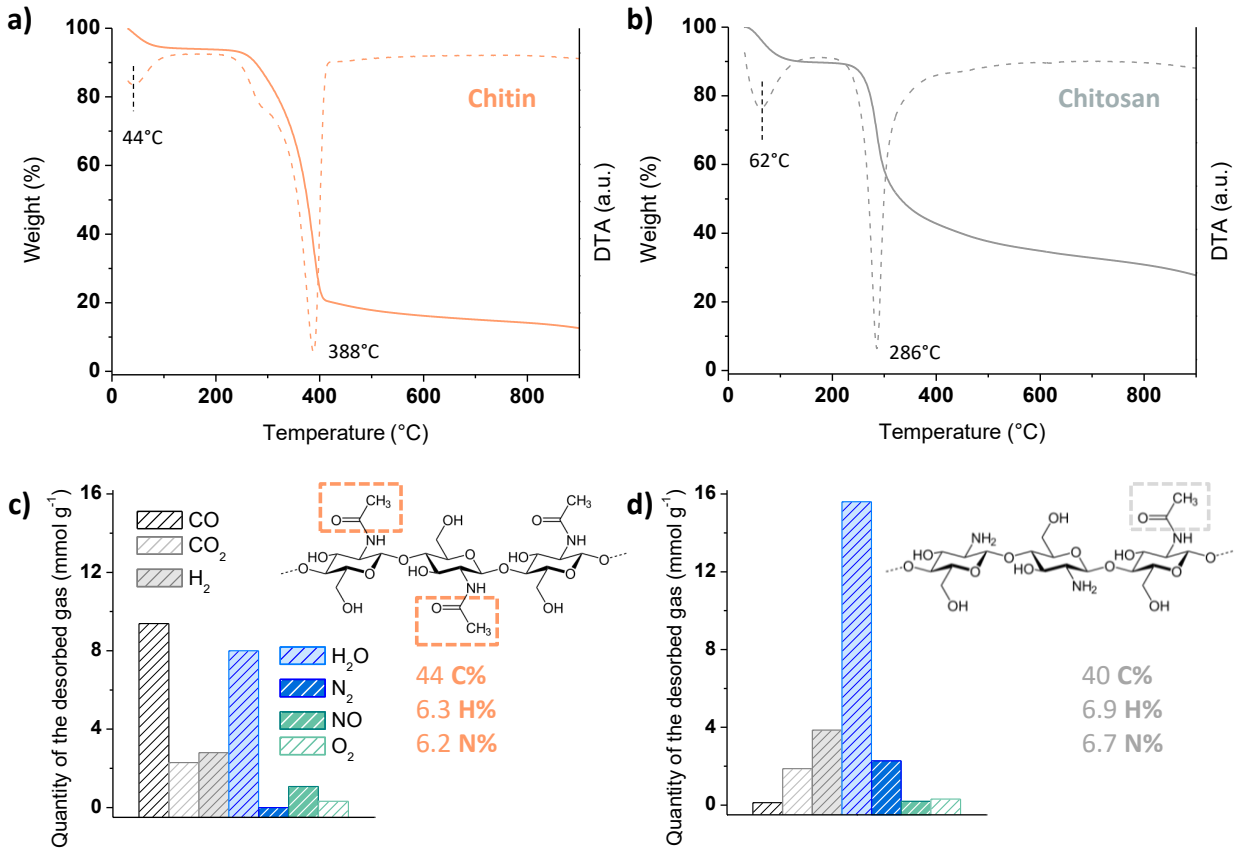

Figure 2 Thermal decomposition of (a) chitin and (b) chitosan studied by TGA. Elemental composition of both bioprecursors and quantities of different gases desorbing from the surface of (c) chitin and (d) chitosan upon heating, analyzed by TPD-MS. The mass spectra collected during the latter experiments can be found in Supporting Information in Figure S1.

A closer look at both materials reveals, however, that although the decomposition of chitin and chitosan takes place in a similar temperature range, the kinetics of this process is dissimilar. While chitin decomposes in one step at around 360°C (Supporting Information, Figure S1a) with the simultaneous release of relatively high amount of CO and H_2O (9.4 and 8.0 mmol g^{-1}, respectively, Figure 2c), and smaller quantities of CO_2, H_2, NO, and O_2 (< 3.0 mmol g^{-1}), its deacetylated counterpart, chitosan, requires two stages to be converted into char. Moreover, its TPD-MS spectrum is mostly dominated by a broad peak of H_2O centered at 280°C (Supporting Information, Figure S1b). Besides the physisorbed water, it might be also the signature of the H_2O originating from the reaction of the two adjacent –OH groups (polycondensation) in chitosan's repeat unit and/or from the dehydration of the two neighboring carboxylic groups.[34, 35] Given the chemical formula of this biopolymer, however, the latter is thought to contribute only to a very small extent to the total amount of released H_2O (16 mmol g^{-1}, Figure 2d). The desorption of other gasses, hidden underneath the peak of H_2O, starts at around 240°C with the release of CO, NO, and O_2 (< 1.0 mmol g^{-1}). It goes through a maximum at around 300°C when CO_2, H_2, H_2O, and N_2 simultaneously desorb from the surface of already partially dehydrated and deaminated chitosan,[36] and continues up to 400-500°C, until the desorption rates of most of the gases decrease to almost zero. The last modification of the char occurs between 500 and 850°C (Supporting Information, Figure S1b).[37, 38] Therein, the carbonization is being completed, the C–H bonds are being cleaved and the structure of carbon rearranges for the last time.

3.2 Bulk and surface properties of hard carbons (HCs)

3.2.1 Porosity and structure

The difference in thermal decomposition of chitin and chitosan has its further consequence in pore formation. As can be seen in Figure 3a and b, processing these two polysaccharides under the same pyrolysis conditions (1300°C, 5°C min^{-1}, under argon) leads to two dissimilar HCs. Significantly larger quantity of N_2 is adsorbed on the surface of HC-cht-1300 than onto its counterpart prepared from chitosan, which, in turn, results in high, as for the application in Na-ion battery, specific surface area (S_{BET}, 110 m^2 g^{-1}). Moreover, the shape of the isotherm measured for this material (type IV) suggests the presence of both micro- and mesopores. The latter seems not to be the case for the other carbon, HC-chs-1300, the isotherm of which resembles that characteristic for non-porous materials with low S_{BET} (here below 10 m^2 g^{-1}). Low S_{BET} holds a promise of reduced electrolyte decomposition and, thus, smaller irreversible loss of specific charge, especially during the first cycle.[39] It is not, however, the one and only performance-defining parameter because HCs with S_{BET} exceeding 10 m^2 g^{-1} have been also identified as strong candidates for negative electrodes for Na-ion batteries.[40] Their electrochemical success in enhancing the performance of this electrochemical system lies, among others, in interconnected network of micro- and mesopores. This network, also referred to as nanoporous, seems to be an important prerequisite for any HC electrode material for Na-ion battery, wherein a part of the charge is stored through pore-filling.[23, 41, 42]

Despite significant difference in total pore volume, V_t (Table 1), the pore size distribution (Figure 3b) is rather similar for both HCs, which besides small mesopores (between 3 to 5 nm) also comprise some micropores (of around 1 nm). In the case of HC-cht-1300, the formation of micropores occupying nearly 30% of the V_t (Table 1) might be related to partial activation of the

char during its annealing, caused by alkali and alkaline metal impurities (mostly Ca) present in the parent material. Possible activation of the HC is believed to involve following reactions:

$$3\,Ca(OH)_2 + 2\,C \rightarrow 2\,CaCO_3 + Ca + 3\,H_2 \quad (4)$$

$$CaCO_3 + C \rightarrow CaO + 2\,CO \quad (5)$$

$$CaO + C \rightarrow Ca + CO \quad (6)$$

similar to those presumably taking place during the classical chemical activation of the carbon-based materials (with KOH).[43, 44] Besides micropores, the pore structure of the chitin-derived HC is also built from ultra-micropores, that is, micropores smaller than 0.7 nm. The volume of the ultra-micropores, $V_{\text{ultra-micro}}$, estimated based on the amount of adsorbed CO_2, is approximately 30% higher than that obtained through N_2 adsorption, indicating significant contribution of these narrow pores to the total S_{BET} of the HC-cht-1300. At the same time, once again it confirms the inability of N_2 to access pores smaller than 1 nm, often mentioned in the literature.[23, 45]

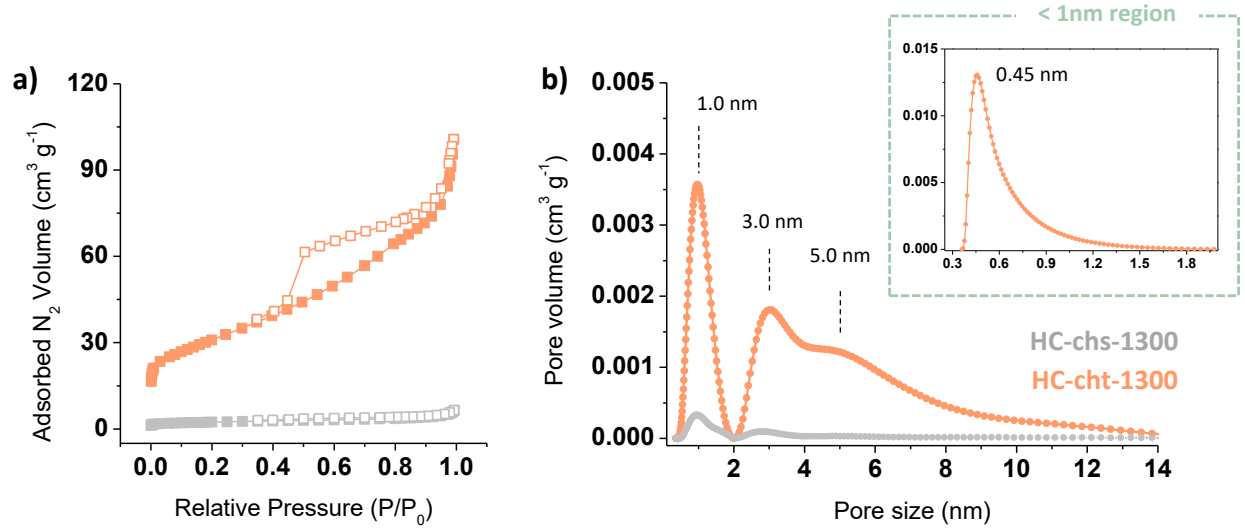

Figure 3 (a) Nitrogen adsorption/desorption isotherms of HC-chs-1300 and HC-cht-1300 and (b) the corresponding NLDFT pore size distributions obtained from the adsorption branches of the N_2 and CO_2 (shown in inset) isotherms. CO_2 adsorption isotherm of HC-cht-1300 can be found in Supporting Information in Figure S2a.

Table 1 Comparison of calculated BET surface areas, total and (ultra-)micropore volumes for the chitin- and chitosan-derived HCs.

	S_{BET} N_2 (m^2 g^{-1})	V_t (cm^3 g^{-1})	V_{micro} (cm^3 g^{-1})	S_{BET} CO_2 (m^2 g^{-1})	$V_{ultra\text{-}micro}$ (cm^3 g^{-1})	d_{002} (Å) L_c (nm)	ASA (m^2 g^{-1})
HC-cht-1300	110	0.156	0.0450	72	0.059	3.61 1.24	11
Non-washed **HC-chs-1300**	2.6	0.005	0.0009	—[1)]	—[1)]	3.65 1.12	1.8
Acid-treated **HC-chs-1300**	3.9	0.007	0.0015	24	0.061	3.62 1.15	5.2

[1)] neither S_{BET} CO_2 nor $V_{ultra\text{-}micro}$ could have been determined for this material. Presumably the number of pores smaller than < 0.7 nm was below the detection limit of the machine, even upon increasing the mass of the sample.

Besides the open pores, chitin- and chitosan-derived HCs also contain pores which are isolated from the external surface and, thus, hardly accessible to electrolyte or any other solvent. The volume of these so-called closed pores, R_{CP} (%), is usually estimated from apparent density (equation (1)). In the case of the chitin-derived HC closed pores account only for 6.4% of the entire volume of the material. The rest of it is composed of open pores (25%) and solid phase (68%). Opposite trend is observed for HC-chs-1300, in which closed and open pores occupy, respectively, nearly 32 and less than 1.0%. These latter values are in line with the recommendation given by Panasonic,[27] according to which the volume ratio of open to closed pores (constituting together with the solid phase sites of Na occlusion and release) should be 30% (or more) to 7% (or less).

Surface area, pore size and its distribution are among the most important factors for the design of the electrode materials.[46] While highly-developed pore-network carries a risk of excessive electrolyte decomposition and substantial loss of charge during the first cycle of the Na-ion cell,[41] reduced porosity may limit the number of available diffusion pathways and adversely affect the wetting of the electrode.[46]

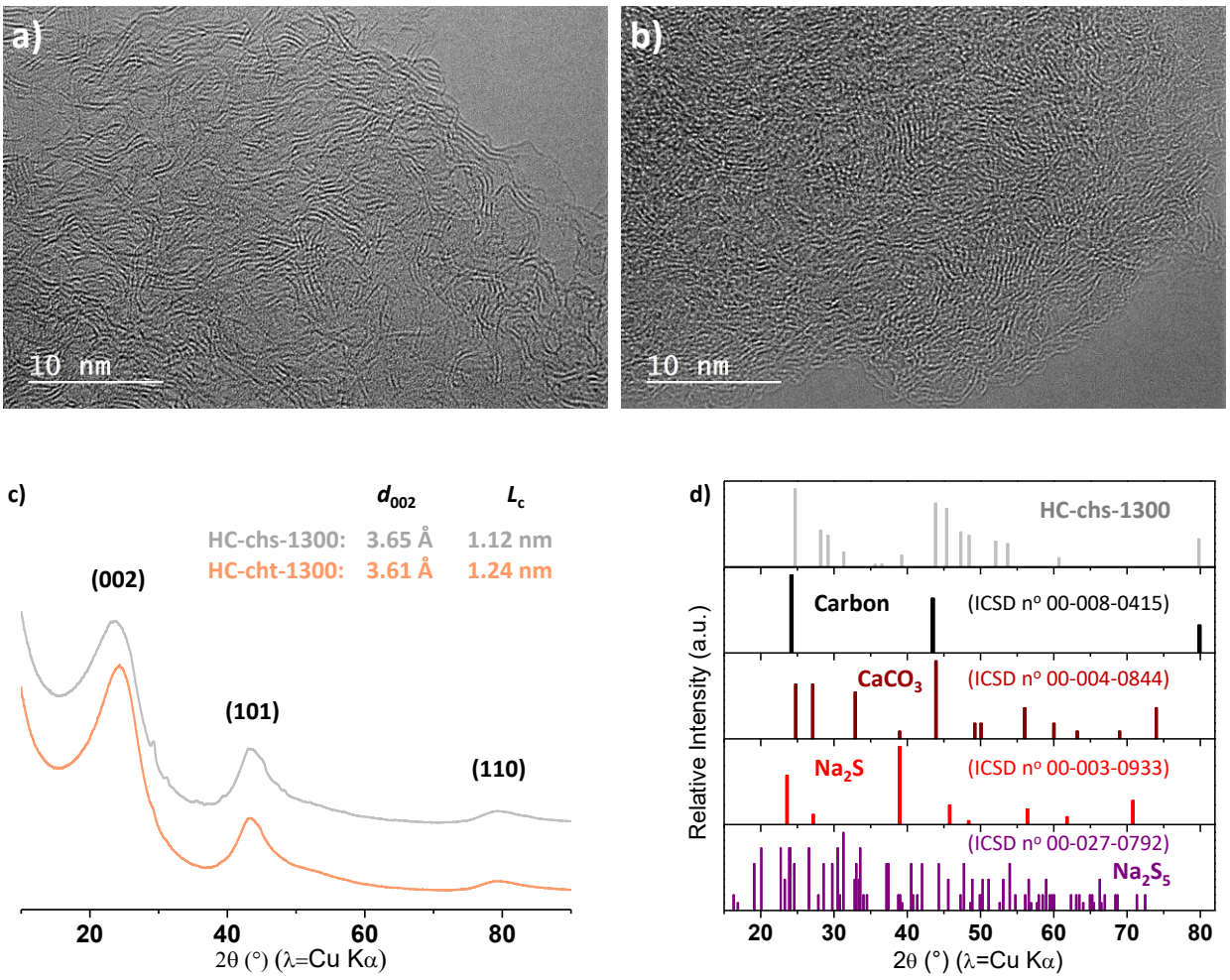

Figure 4 HRTEM images of a) chitin- and b) chitosan-derived HCs. c) XRD patterns of the two hard carbons together with the calculated interlayer spacing, d_{002}, and crystallite size, L_c. d) Possible signatures of the impurities identified in the ICSD database for the HC-chs-1300.

Moreover, because sodiation (and de-sodiation) of HC is not a single-stage process,[41] diffusion of Na-ions into the bulk of the electrode material is only a half of the energy-storage battle. Therein, the "organization" of inherently disordered and irregular microstructure of HC[47] will either promote or impede the insertion of Na-ions between the carbon layers in graphitic domains. To facilitate the sodiation of HC the distance between these layers (referred to as d_{002}) should be higher than that in graphite (3.4 Å),[39, 41] ideally close to 3.7 Å,[48] and the degree of structural disorder should exceed 1, if calculated as an intensity ratio of the disorder (D) and graphitic (G) Raman bands.[41]

As can be seen in Figure 4, these requirements seem to be fulfilled for both biopolymer-derived HCs, HC-cht-1300 and HC-chs-1300, in the overall amorphous structure of which one can distinguish short-range spatially organized nanodomains with the average d_{002} of 3.63 Å, curved graphene nanosheets, and empty voids between them.[49] However, while the honeycomb-like features can be well-seen in the TEM image of HC-cht-1300 (and resemble those reported in ref [50]), they cannot be found in the microstructure of chitosan-derived HC. Instead, lower-magnification TEM pictures reveal dual microstructure of this HC (Supporting Information, Figure S4), in which disordered-like regions, typically observed for HCs, interwind with graphitic layers linked with closed pores.

3.2.2 Impurities

Successful reversible storage of Na-ions in HC depends very much not only on its structure and texture, but also on the presence of impurities. According to the XPS analysis (Table 2), chitosan-derived HC contains calcium, presumably in the form of $CaCO_3$, (Figure 4d), sodium, and sulfur (bonded together in Na_2S and/or its derivatives (Na_2S_4 or Na_2S_5, Figure 4d), all of which significantly reduce the carbon-content of this material. While the amount of Na and S detected

by this surface-sensitive technique is below 1.0 at%, that of Ca reaches almost 4.4 at%. Given the average depth of the XPS analysis (typically not exceeding 10 nm), one could expect different amount (and distribution) of $CaCO_3$ in the bulk of the HC-chs-1300. The latter cannot be, however, quantitatively confirmed by means of SEM-EDX because of the non-homogenous distribution of $CaCO_3$ in the material causing local sample charging followed by a sharp decrease in the number of counts (Figure 5). It seems, however, that the $CaCO_3$ impurities are mainly located at the edges of the carbon particles (inset in Figure 5b) and to lower extent on their surfaces. The presence of this electrically insulating carbonate onto chitosan-derived HC may lead to a decrease in the overall conductivity of this material as well as partially or entirely block some of the Na-ion pathways inside the electrode, therefore altering the local and macroscopic transport properties.

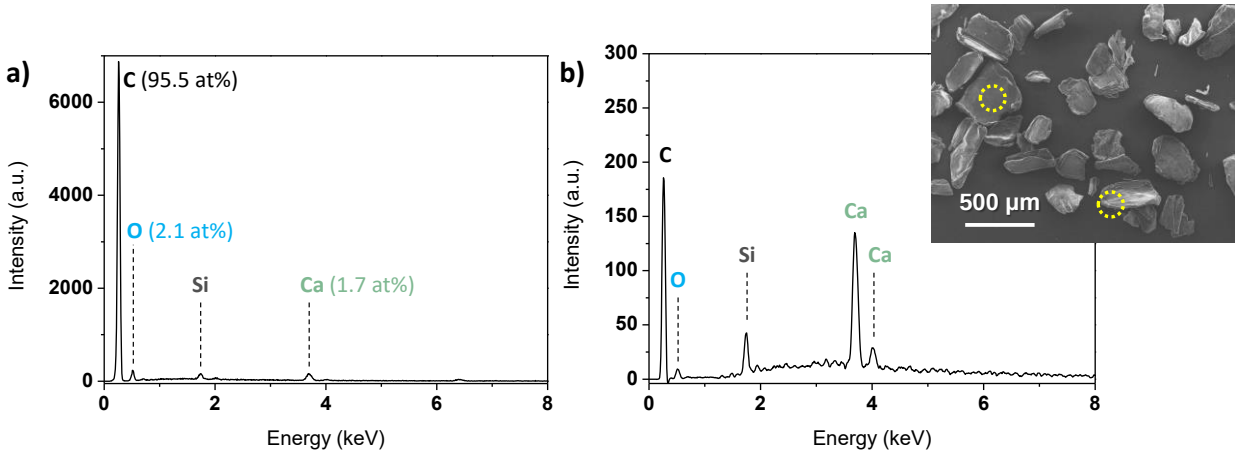

Figure 5 EDX spectra of HC-chs-1300 recorded (a) at the surface (on top of the carbon sheet) and (b) at the edge of the carbon particle (in between the carbon sheets) as marked in the inset SEM image in (b).

Table 2 Overview of the chemical composition of the surfaces of non-washed and acid-treated chitosan-derived HCs and the surface of chitin-derived HC analyzed by XPS.

Atomic %	**C 1s**	**Ca 2p**	**N 1s**	**Na 1s**	**O 1s**	**S 2p**	**Cl 2p**
HC-cht-1300	96.2	1.0	—	—	2.8	—	—
Non-washed **HC-chs1300**	78.9	4.3	0.7	0.7	14.9	0.3	—
Acid-treated **HC-chs-1300**	92.4	0.3	0.3	—	6.0	0.2	0.3

Unlike Na_2S (and its derivatives), $CaCO_3$ has a very low solubility in water (0.015 g L^{-1} at room temperature), unless it is saturated with CO_2 and/or its pH approaches (or exceeds) ~ 5.6. In the latter case, $CaCO_3$ forms bicarbonate, which is more soluble in water (160 g L^{-1} at room temperature) and, thus, easier to be washed away. Besides CO_2-saturated water, hydrochloric acid, HCl can be used as well to purify chitosan-derived HC. In general, the efficiency of Ca removal from the carbon is estimated between 80 and 95%, depending on the amount and distribution of this impurity in the material, the duration of the acid washing, and the efficiency of carbon-acid mixing (dissolution rate of Ca salt within carbon pores).[25] 4 at% of Ca found only on the surface of HC-chs-1300 (Table 2) is already considered as high Ca loading and, thus, requires the use of HCl with the concentration exceeding 5%.

Washing HC-chs-1300 with a fairly concentrated HCl resulted in significant decrease of the amount of Ca and O on the surface (and in the bulk, Supporting Information, Figure S5) of the HC-chs-1300 (from 4.3 to almost 0 at% and from 14.9 to 6 at%, respectively, Table 2), and the disappearance of the Bragg peaks at 29.3, 35.6, 39.4, 47.2, and at 48.3° (Supporting Information, Figure S6). Moreover, the small quantity of Na also initially present on the surface of this HC most probably in the form of sulfide(s) is no longer detected after the acid-treatment.

Unfortunately, the use of this inorganic acid leaves behind some residual chloride ions in the pores of carbon (Table 2), which might be released into the electrolyte during cycling and obscure the true electrochemical performance of this material.

The removal of both $CaCO_3$ and Na_2S, and/or its derivatives, has its further consequence on the N_2 BET surface area, S_{BET} N_2, which increases from 2.6 $m^2 g^{-1}$ for the non-washed sample to 3.9 $m^2 g^{-1}$ for the sample treated with HCl (Supporting Information Figure S3 and Table 1). Based on the pore volume analysis (and measured S_{BET} CO_2, Supporting Information Figure S2 and Table 1**)**, we assume that the observed increase in S_{BET} might be either due to i) the development of some additional micropores and/or opening of the pores previously clogged by inorganic contaminants,[51] or ii) the etching of the hard carbon with fairly concentrated acid, or both.

Contrary to the chitosan-derived HC, the carbon prepared from chitin is mostly free from impurities (less than 1 at% of Ca detected by XPS, and no traces of Na and S, Table 2) and contains significantly less oxygen (2.8 *versus* 14.9 at% for the non-washed HC-chs-1300, Table 2), at least on its surface. The difference in chemical composition of the chitin- and chitosan-derived HC may stem from the difference in the amount and distribution of Ca and other inorganic residuals in respective parent material. While the amount of $CaCO_3$, a crustacean shell stiffening agent, in chitin varies with species, season and environmental growth conditions,[52] its residual amount in HC might be linked to migration of this impurity towards the surface of carbon forming during the thermal treatment. Once the melting point of Ca is exceeded (842°C), some of the Ca "sitting" at and/or near the surface of the material might be removed, while others originally located more in the bulk may remain therein and be oxidized to carbonates upon contact with air (while being taken out from the furnace). Moreover, although HC-cht-1300 has

been prepared from the precursor rich in nitrogen (Figure 2c), it seems not to be doped with this heteroatom, which might be related to the temperature of the thermal treatment (1300°C) favoring the removal of nitrogen and other dopants from the structure of carbon.[53] Lowering this temperature could result in N-doped HC, as it was the case of the materials prepared by Hao *et al.*,[54] however, with the sacrifice of most of the important physicochemical properties, such as for example S_{BET} and electrical conductivity.

3.2.3 Surface chemistry

In Na-ion battery, as in any other energy storage system, the surface chemistry of carbon is equally, if not more, important that the bulk properties of this material. This is because sodium storage mechanism in HC relies not only on its intercalation into graphitic nanodomains but also on surface reactions and formation of Na clusters in the pores and at the edges of carbon.[41] According to recent studies[23, 53, 55] the two latter influence mostly the high-potential charge storage behavior of HC and define its reactivity towards the electrolyte and, thus, the extent of the electrolyte decomposition during the first cycle.

Based on the TPD-MS analysis (Figure 6) it seems that the surface of HC-cht-1300 is much richer in functional groups than that of its chitosan-derived counterpart, which together with the higher S_{BET} may favor the electrolyte decomposition. Moreover, some of these groups, for example carboxyl groups, have been previously reported as "electrochemically inactive"[56] and, thus, their presence on the surface of carbon may impede the charge transfer to and between the particles. The electrochemical behavior of these and other available functional groups will, however, depend on the environment (the electrolyte), the electrode engineering (selection of binder and solvent for electrode formulation), and the applied testing conditions.

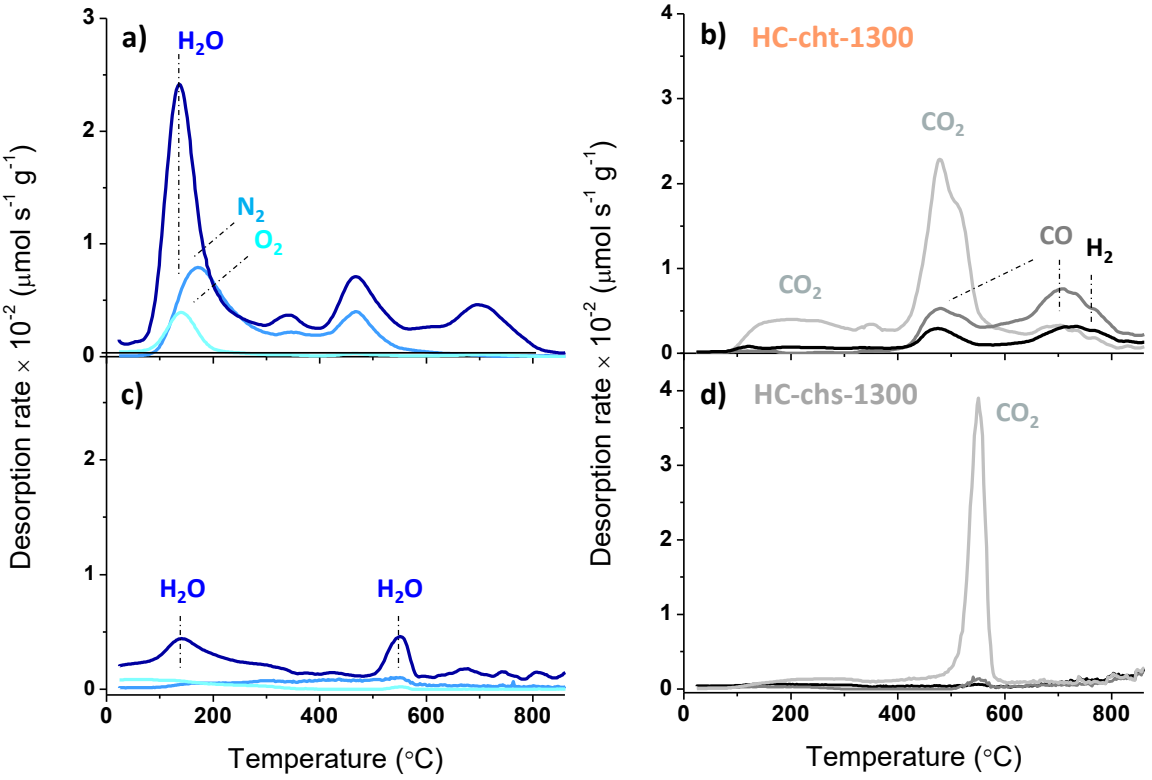

Figure 6 TPD-MS spectra collected for (a, b) chitin- and (c, d) chitosan-derived HCs. For clarity the spectrum of each HC was split into two graphs: (a and c) one showing only the evolution of H_2O, N_2, and O_2, and (b and d) the second graph presenting the desorption profiles of CO_2 and other detected gases.

At low temperature the TPD-MS spectra of chitin- and chitosan-derived HCs are mainly dominated by H_2O. The amount of water, O_2 and N_2 desorbing from the surface of HC-cht-1300 at 140°C is, however, twice as high as that from HC-chs-1300 (0.10 mmol g^{-1} *versus* 0.04 mmol g^{-1}, respectively, Figure 7), most probably because of some moisture (and air) trapped in the micropores of the former material. Given that the drying temperature of the carbon-based slurry typically does not exceed 80°C, this water may remain in the pores of HC-cht-1300 and

block their passage for Na-ions. It may also promote some undesired side reactions with the electrolyte.

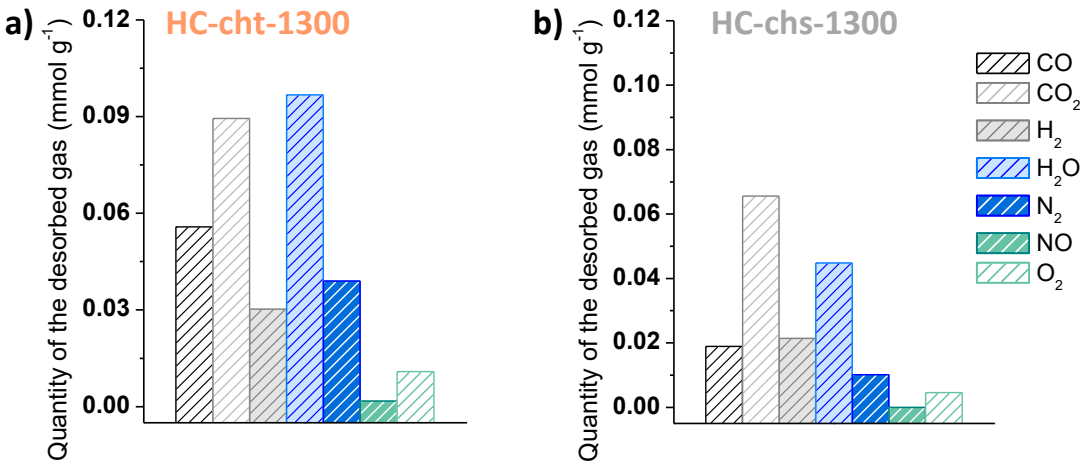

Figure 7 Quantities of different gases desorbing from the surface of (a) chitin- and (b) chitosan-derived HCs upon heating, analyzed by TPD-MS.

The H_2O peak observed at around 470°C presumably originates from structurally bound water (chemisorbed water) and perhaps also from some inorganic carbonates, decomposing at higher temperatures to CO and CO_2 (Figure 6b). Moreover, the peak appearing in the TPD-MS spectrum of HC-cht-1300 shortly before the temperature reaches 500°C originally assigned to N_2 might be in fact a signature of CO (Figure 6a). Given identical mass-to-charge ratio (m/z = 28) of these two molecules, it is often difficult to differentiate between CO and N_2 signals in the MS spectrum and correctly assign their contributions.

The desorption of CO_2 from the surface of chitin-derived HC begins at 200°C and covers almost entire experimental temperature range, suggesting a great variety of oxygen-containing functional groups present onto this carbon. In addition, the TPD-MS profile of CO_2 can be divided into two

regions, low and medium temperature regions, and analyzed based on the classification widely accepted in the literature.[57] One has to note, however, that the desorption profiles recorded for HCs prepared either from biowastes (also biopolymers) or phenolic resins[22] often differ from those observed for (modified) commercial carbons and, thus, some of the peaks cannot be assigned unequivocally to the specific oxygen-containing surface groups. Nevertheless, in the case of HC-cht-1300 the broad CO_2 peak in the low temperature region between 100 and 300°C without any apparent maximum could be associated with the decomposition of carboxyl groups.[57] Next, the peak centered at around 480°C presumably corresponds to carboxylic anhydrides because at this temperature CO_2 desorbs together with its monoxide counterpart, CO (Figure 6b). It might be also a signature of carbon impurities, inorganic carbonates, mentioned earlier in the text. Besides carboxyl, and carboxylic anhydrides the surface of the chitin-derived carbon seems to be also composed of lactones. These cyclic esters, thermally more stable than carboxylic anhydrides, usually leave the structure of carbon at higher temperatures and often form a shoulder somewhere between 500 and 600°C.[57] The contribution of the CO_2 observed above 600°C does not come from the surface functional groups. As shown by Frost *et al.*,[58] and later also by Ghimbeu and co-workers,[59] it is rather linked to the decomposition of inorganic carbonate(s), M_xCO_3 (here mostly $CaCO_3$), to M_xO (CaO). Finally, the CO peak appearing at the end of the TPD-MS spectrum of this HC (600 – 800°C) indicates the presence of ether, phenol, and/or quinone groups, whereas that of H_2 is most probably related to the cleavage of C – H bonds and subsequent organization of the carbon structure.

As already mentioned, significantly smaller amount of (physi- and chemisorbed) water is released from HC derived from chitosan, HC-chs-1300 (Figure 7). Moreover, because the CO_2 desorbs at the temperature higher than 500°C and gives rise to a well-defined sharp peak it might

correspond to the thermal decomposition of one of the HC-chs-1300 impurities, namely $CaCO_3$, rather than the carboxyl groups present on its surface (Figure 6d). Once this peak disappears from the TPD-MS spectrum of HC-chs-1300 no other signal appears therein, further confirming "poor" surface chemistry of this material.

Acid-treatment leads to some changes in the TPD-MS spectrum of the chitosan-derived HC (Supporting Information Figure S7a). Much less CO_2 (and CO) is released from the HC-ch-1300 treated with HCl (Supporting Information Figure S7b) than from its non-washed counterpart (0.03 mmol g^{-1} *versus* 0.07 mmol g^{-1}, respectively), further confirming successful removal of inorganic impurities from the structure of this HC.

TPD-MS not only provides information about the surface chemistry of the HCs but also about the active surface area (ASA), which is perhaps the most critical parameter in engineering of the carbon-based electrodes.[46] ASA, usually determined by oxygen chemisorption at 300°C, represents the edge planes and the defects developed in carbon edge planes — the active sites,[60] and can be used as an index of carbon reactivity towards the electrolyte and other ions. If so, chitin-derived HC with much larger active surface area should have significantly higher "electrochemical reactivity" than its counterpart prepared from chitosan (11 m^2 g^{-1} *versus* 1.8 m^2 g^{-1}, respectively; the ASA of graphite usually falls below 1 m^2 g^{-1}).[61] Moreover, because the active surface area is inversely proportional to the width of graphitic domains (along ab planes),[41, 62, 63] we also assume more reversible Na-ion storage in HC-cht-1300. The smaller the width of these domains, the more crystalline the material (more "organized") and, thus, the lower the specific charge expected from low-potential plateau of sodiation profile (typically observed between 0.10 and 0.05 V).

The ASA of HC-chs-1300 increases upon acid-treatment (from 1.8 to 5.2 $m^2 g^{-1}$, respectively), most probably mainly as a consequence of micropore formation and/or pore-unblocking, and to a lesser extent due to the changes in surface chemistry. Moreover, as it was shown in the previous section, acid-treatment of the HC-chs-1300 leads to the removal of inorganic impurities and, thus, a significant increase in the carbon content of this material (from 78.9 to 92.4 at%, Table 2), contributing to greater ASA.

3.2.4 Electrochemical performance

Next, chitin- and chitosan-derived HCs were tested in half cells versus sodium metal. As can be seen in Figure 8, both negative-electrode materials attained almost 280 mAh g^{-1} during the first desodiation. However, while in the case of the chitin-derived HC this value is presumably a sum of excessive electrolyte decomposition onto the external surface of this carbon (relatively large S_{BET}) compensated by low content of inorganic impurities, and presence of mesopores, similar capacity attained for the cell assembled with HC-chs-1300-based electrode is a result of low S_{BET} ("restrained" electrolyte decomposition) and partial insulation of the surface by impurities (mainly Ca, impeded charge percolation and its transfer to and within the electrode) counterbalanced by Na occlusion in and release from closed "graphitic" pores. [27]

A closer look at the galvanostatic profiles of the first few cycles of the chitin- and chitosan-derived HCs further clarify the Na-ions storing mechanism in these two materials (Supporting Information, Figure S8a-c). It should be mentioned, however, that the debate about the mechanism of Na-ion storage in hard carbons and the assignment of the features observed in galvanostatic profiles of the Na-ion continues until this day.

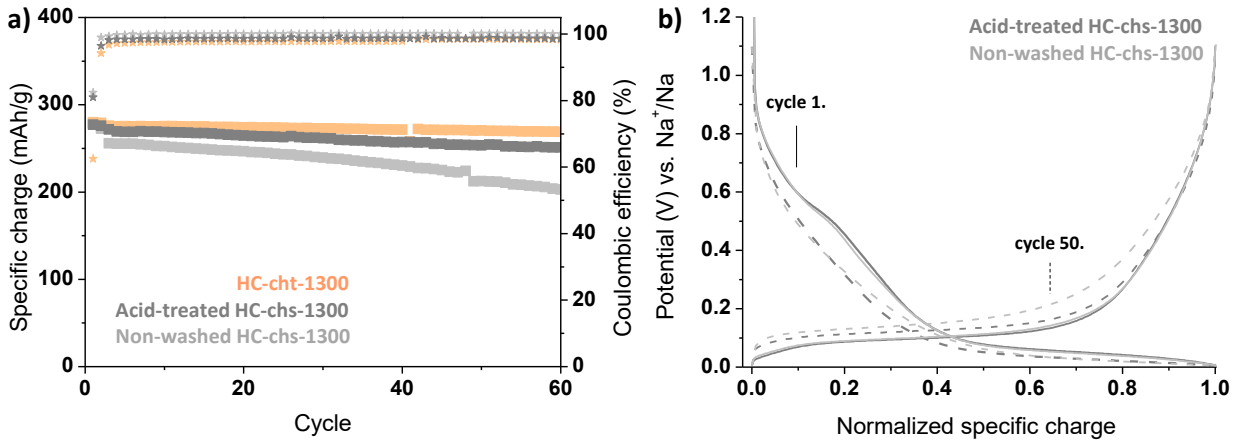

Figure 8 (a) Specific charge (squares) and Coulombic efficiency (stars) of the Na-ion half-cells tested with electrodes based on chitin- and chitosan-derived HCs. For clarity, only the specific charge obtained during charge (desodiation) is presented in the graph. (b) Evolution of the polarization during 1st and 50th cycle for the cells assembled with the electrodes based on non-washed and acid-treated HC-chs-1300.

In some studies, the slope and the plateau regions are attributed, respectively, to mesopore filling/adsorption of Na-ions within micropores and their insertion into graphitic domains, while the other reports claim exactly the opposite. Moreover, besides the wide-range of physicochemical properties, the ease and extent of the SEI formation onto HC seems also to have its large share in defining cycling stability and reversibility of the sodiation/desodiation processes.

During the first cycle the shape of the galvanostatic curve varies significantly depending on the HC-based electrode used in the cell (the derivatives of the galvanostatic curves can be found in Supporting Information, in Figure 8e-g). A “shoulder” between 0.6 and 0.2 V vs. Na^+/Na, often ascribed to SEI formation, is more pronounced in the case of HC-cht-1300 than in the case of its counterparts prepared from chitosan (non-washed and acid-treated). This observation is in good

agreement with the S_{BET} and ASA values, both of which are significantly higher for HC-cht-1300 (Table 1). It also explains much lower first-cycle Coulombic efficiency (CE) found for the cell assembled with this HC (62% *versus* 82% obtained for the HC-chs-1300). Higher amount of charge consumed for the SEI formation does not necessarily limit the performance of the HC-cht-1300. Instead, in the long run, it brings about slightly higher reversible capacity and better cycling stability.

The slope-region between 1.0 and 0.1 V, more visible from the second cycle onwards, could be attributed to the adsorption of Na-ions within micropores.[64] Therein, judging from V_{micro} (Table 1) the chitin-derived HC should outperform the non-washed chitosan-derived HC. This is not, however, the case as can been seen in Figure S8b, in Supporting Information. Apparently, storing the Na-ions in the chitosan-derived HC does not proceed through their adsorption in micropores (very limited in this material, Table 1) and the specific charge gained along the slope originates from yet another storing behavior. The latter, according to the literature,[27] might be related to adsorption of Na-ions in closed "graphitic" pores. Usually these pores start to form once the temperature of the thermal treatment exceeds 2000°C.[53] However, it is possible that inorganic impurities present in chitosan (and residing in forming HC) lower the graphitization temperature,[65] therefore triggering pore closure. These initially isolated pores may partially open up during the first sodiation due to some small volume changes of the carbon particles, causing mechanical stress to the active material and, thus, creating additional sites for Na insertion. Finally, Na adsorption in the vicinity of an oxygen- (nitrogen-) and vacancy-containing defect sites in HC-chs-1300 might also contribute to the amount of specific charge gained along the slope-region of the sodiation process.[66]

As for the plateau region, more and more often ascribed to the Na-ions insertion into graphitic domains, we do not notice significant changes depending on the HC used as an active material (at least not in the early stage of cycling), except for slightly longer potential-plateau for HC-chs-1300. This presumably stems from a bit larger d_{002} found for this material (Table 1). Furthermore, slightly higher IR drop observed for the cell with HC-chs-1300 compared to that with HC-cht-1300 most probably is a result of less stable SEI formed onto the former HC and the presence of oxygen-rich inorganic impurities rendering the surface of this carbon partially insulating.

Removal of $CaCO_3$ and other impurities (Na_2S and/or its derivatives) from the structure of chitosan-derived HC (acid-treated) causes the IR drop to decrease (Figure 8b). It also leads to the improvement in cycling performance of this HC, which almost coincides with that of chitin-derived HC. Moreover, enhanced specific charge retention in the case of the acid-treated HC-chs-1300, reaching almost 96% (only 79% reversibility in the case of non-washed sample), could be triggered by a better balance between the carbon content (an increase from 78.9 to 92.4 at% after washing, Table 2), bulk porosity and surface chemistry of this material.

Finally, the average reversible specific charge of 260 mAh g^{-1} found for HCs derived from chitin and (acid-treated) chitosan is close to the values reported for HCs prepared from their structural analogue, cellulose (Table 3).

Table 3 Electrochemical performance of reported HC derived from cellulose.

HC precursor	**Loading** (g cm^{-2})	**Electrolyte formulation**	**Potential window** (V)	**Specific charge** (mAh g^{-1})	**Ref**
reagent-grade **saccharide**	not specified	1M $NaPF_6$ in PC	0.002–2.0	353 at C/20	[15]
microcrystalline **cellulose powder**	not specified	1M $NaPF_6$ in EC/DMC	0.010–3.0	300 at C/10	[67]
filter paper	not specified	1M $NaClO_4$ in EC/PC	0.010–3.0	280 at	[68]

				~ C/25	
Cellulose **filter paper**	1.0–1.5	1M $NaPF_6$ in EC/DEC	0.010–2.0	308 at ~ C/25	[69]
Chitin /Acid-treated chitosan	6.0	1M $NaPF_6$ in EC/DEC	0.010-1.1	260 at C/5	This work

Unfortunately, due to the discrepancies in active-material loading (if specified), electrolyte formulation, operating potential window, and applied current (C-rate), more accurate comparison with other studies on HCs for Na-ion battery cannot be made. Nevertheless, reversible 260 mAh g^{-1} attained for nearly 6 mg-loaded electrodes subjected to higher currents during sodiation/desodiation (C/3) speak in favor for further development of negative-electrode materials based on chitin (or acid-treated chitosan).

4. Conclusions

To sum up, pyrolysis of two structurally similar bioprecursors, namely chitin and chitosan, yields dissimilar hard carbons in terms of porosity, surface chemistry and the presence of impurities (mainly $CaCO_3$). The latter can be removed from the material by simple acid-treatment without adversely affecting its structural and textural properties, as we showed on the example of chitosan-derived HC. Also, it can be beneficial for unblocking some of the micropores and enhancing the active surface area of the material.

HCs prepared from biopolymers or any other parent materials for energy storage applications very often required additional post-thermal treatment(s) and/or further tuning of their morphology, structure, and texture. These optimization of carbon properties should be always carried out stepwise, with little/no harm to its other physicochemical characteristics to still enable drawing a comparison between the optimized and the reference materials and identifying

remaining weak points. Moreover, even if continuous pursuit of high-capacity negative electrode materials for Na-ion battery imposes quick screening of possible candidates, this screening should be always accompanied by a thorough characterization of the material (and its precursor) to better foreseen its electrochemical performance and related limitations. Based on the results presented here we conclude that rich surface chemistry and micro-mesoporous texture of the chitin-derived HC promotes excessive decomposition of the electrolyte, leading to low first-cycle Coulombic efficiency. It does not, however, exclude a good cycling stability, further supported by low content of inorganic impurities. Less electrolyte decomposition seems to plague non-porous chitosan-derived HC, which, in turn, suffers from lower cycling stability caused by alkali and alkaline metal-containing impurities, rendering its surface partially insulating. The latter limitation can be overcome by acid-washing, which is an effective remedy to tame continuously declining specific charge.

Supporting Information. TPD-MS spectra of chitin and chitosan; Textural characterization of chitin- and chitosan-derived HCs (also acid-treated material); Changes in morphology, structure, and surface chemistry of the HC-chs-1300 as a function of the post-processing, that is, removal of the impurities; Potential profiles and corresponding first derivative of the galvanostatic curves for all tested HCs.

Acknowledgements

The authors would like to thank G. Schrodj, B. Rety and Dr. J. Denzer for TGA and TPD-MS experimental support and countless hints for the data analysis. In addition, we would like to acknowledge Dr. L. Vidal, J.-M. Le Meins and Dr. P. Fioux for, respectively, TEM, XRD and XPS measurements performed through technical platforms available at IS2M. This work was

performed within the framework of RS2E network and the laboratory of excellency for electrochemical energy storage, STORE-EX, and financed by European Union's Horizon 2020 Program (project NAIADES, call: LCE10-2014, Contract no. 646433).

References

(1) Dutta, P. K.; Dutta, J.; Tripathi, V. S. Chitin and chitosan: Chemistry properties and applications. *J. Sci. Ind. Res.* **2004,** *63*, 20-31.
(2) Aranaz, I.; Mengibar, M.; Harris, R.; Miralles**,** B.; Acosta, N.; Calderon, L. Role of Physicochemical Properties of Chitin and Chitosan on their Functionality. *Curr. Chem. Biol.* **2014,** *8*, 27-42.
(3) Huang, L.; Xiao, L.; Yang, G. Chitosan Application in Textile Processing. *Curr. Trends Fashion Technol. Textile Eng.* **2018,** *4* (2), 555635.
(4) Bano, R. Use of Chitosan in Mosquito Repellent Finishing for Cotton Textiles. *J. Textile Sci. Eng.* **2014,** *4* (5).
(5) Shakeel, A.; Saiqa, I. Chitosan Based Scaffolds and Their Applications in Wound Healing. *Achievements in the Life Sciences* **2016,** *10* (1), 27-37.
(6) RSS Print, 4 materials which are the future of medtech https://www.med-technews.com/latest-issue/4-materials-which-are-the-future-of-medtech/ (accessed Oct 1, 2018).
(7) Hecht, J. Shrimp-shell wound healant to get space test https://www.newscientist.com/article/dn12361-shrimp-shell-wound-healant-to-get-space-test/ (accessed Oct 1, 2018).
(8) Kolodziej, A.; Fic, K.; Frackowiak, E. Towards sustainable power sources: chitin-bound carbon electrodes for electrochemical capacitors. *J. Mater. Chem. A* **2015,** *3*, 22923-22930.
(9) Jie, Z.; Li, B.; Shengji, W.; Wei, Y.; Hu, W. One-step synthesis of chitin-derived nitrogen-rich porous carbon fiber assisted with ammonium chloride chemical blowing for supercapacitors. *J. Mater. Sci.: Mater. El.* **2018,** *29* (14), 12340-12350.
(10) Duan, B.; Gao, X.; Yao, X.; Fang, Y.; Huang, L.; Zhou, J. Unique elastic N-doped carbon nanofibrous microspheres with hierarchical porosity derived from renewable chitin for high rate supercapacitors. *Nano Energy* **2016,** *27*, 482-491.
(11) Yan, L.; Yu, J.; Huston, J.; Flores, N.; Luo, H. Biomass derived porous nitrogen doped carbon for electrochemical devices. *Green Energy & Environment* **2017,** *2* (2), 84-99.
(12) Cao P.-F.; Naguib, M.; Du, Z.; Stacy, E.; Li, B.; Hong, T. Effect of Binder Architecture on the Performance of Silicon/Graphite Composite Anodes for Lithium Ion Batteries. *ACS Appl. Mater. Interfaces* **2018,** *10* (4), 3470-3478.
(13) Chao, C.; Sang, H. L.; Misuk, C.; Jaehoon, K.; Youngkwan, L. Cross-Linked Chitosan as an Efficient Binder for Si Anode of Li-ion Batteries. *ACS Appl. Mater. Interfaces* **2016,** *8* (4), 2658-2665.
(14) Śliwak, A.; Díez, N.; Miniach, E.; Gryglewicz, G. Nitrogen-containing chitosan-based carbon as an electrode material for high-performance supercapacitors. *J. Appl. Electrochem.* **2016,** *46* (6), 667-677.

(15) Yamamoto, H.; Muratsubaki, S.; Kubota, K.; Fukunishi, M.; Watanabe, H.; Kim, J. Synthesizing higher-capacity hard-carbons from cellulose for Na- and K-ion batteries. *J. Mater. Chem. A* (35), 16844-16848.
(16) Stevens, D. A.; Dahn, J. R. High Capacity Anode Materials for Rechargeable Sodium-Ion Batteries. *J. Electrochem. Soc.* **2000,** *147* (4), 1271-1273.
(17) Irisarri, E.; Amini, N.; Tennison, S.; Ghimbeu, C. M.; Gorka, J.; Vix-Guterl, C. Optimization of Large Scale Produced Hard Carbon Performance in Na-Ion Batteries: Effect of Precursor, Temperature and Processing Conditions. *J. Electrochem. Soc.* **2018,** *165* (16), A4058-A4066.
(18) Li, Y.; Hu, Y.-S.; Li, H.; Chen, L.; Huang, X. Y. A superior low-cost amorphous carbon anode made from pitch and lignin for sodium-ion batteries. *J. Mater. Chem. A* (1), 96-104.
(19) Hasegawa, G.; Kanamori, K.; Kannari, N.; Ozaki, J.-I.; Nakanishi, K.; Abe, T. Studies on electrochemical sodium storage into hard carbons with binder-free monolithic electrodes. *J. Power Sources* **2016,** *318*, 41-48.
(20) Li, Y.; Mu, L.; Hu, Y.-S.; Li, H.; Chen, L.; Huang, X. Pitch-derived amorphous carbon as high performance anode for sodium-ion batteries. *Energy Storage Materials* **2016,** *2*, 139-145.
(21) Saurel, D.; Orayech, B.; Xiao, B.; Carriazo, D.; Li, X.; Rojo, T. From Charge Storage Mechanism to Performance: A Roadmap toward High Specific Energy Sodium-Ion Batteries through Carbon Anode Optimization. *Adv. Energy Mater.* **2018,** *8* (17), 1703268.
(22) Beda, A.; Taberna, P.-L.; Simon, P.; Ghimbeu, C. M. Hard carbons derived from green phenolic resins for Na-ion batteries. *Carbon* **2018,** *139*, 248-257.
(23) Ghimbeu, C. M.; Górka, J.; Simone, V.; Simonin, L.; Martinet, S.;Vix-Guterl, C. Insights on the Na+ ion storage mechanism in hard carbon: Discrimination between the porosity, surface functional groups and defects. *Nano Energy* **2018,** *44*, 327-335.
(24) https://www.freepik.com/free-vector/shrimp-icon_761754.htm#term=shrimp&page=1&position=0 (accessed Oct 1, 2018).
(25) Marsden, J.; House, I. *The Chemistry of Gold Extraction*, Society for Mining, Metallurgy, and Exploration, Inc.: Colorado, **2006**.
(26) Jagiello, J.; Olivier, J. P. Carbon slit pore model incorporating surface energetical heterogeneity and geometrical corrugation. *Adsorption* **2013,** *19* (2), 777-783.
(27) Kano, A.; Hojo, N.; Fujimoto, M. Negative-electrode active material for sodium-ion secondary battery, method for manufacturing said negative-electrode active material, and sodium-ion secondary battery. US Patent 2016/0104889 **2016**.
(28) Warren, B. E. X-Ray Diffraction Study of Carbon Black. *J. Chem. Phys.* **1934,** *2* (9), 551-555.
(29) Warren, B. E. X-Ray Diffraction in Random Layer Lattices. *Phys. Rev.* **1941,** *59* (9), 693.
(30) Kercher, A. K.; Nagle, D. C. Microstructural evolution during charcoal carbonization by X-ray diffraction analysis. *Carbon* **2003,** *41* (1), 15-27.
(31) Jian, K.; Trung, T. C.; Hoffman, W. P.; Hurt, R. H. Mesoporous carbons with self-assembled high-activity surfaces. *Microporous Mesoporous Mater.* **2008,** *1* (108), 143-151.
(32) Laine, N. R.; Vastola, F. J.; Walker, P. L. The Importance of Active Surface Area in the Carbon-Oxygen Reaction1,2. *J. Phys. Chem.* **1963,** *67* (10), 2030-2034.
(33) Conder, J.; Villevieille, C. How reliable is the Na metal as a counter electrode in Na-ion half cells? *Chem. Commun.* **2019,** *55*, 1275-1278.
(34) Brender, P.; Gadiou, R.; Rietsch, J.-C.; Fioux, P.; Dentzer, J.; Ponche, A. Characterization of Carbon Surface Chemistry by Combined Temperature Programmed Desorption with in Situ X-

ray Photoelectron Spectrometry and Temperature Programmed Desorption with Mass Spectrometry Analysis. *Anal. Chem.* **2012,** *84* (5), 2147-2153.
(35) Takafumi, I.; Takashi, K. In *Materials Science and Engineering of Carbon*; Inagaki, M.; Kang, F., Eds.; Elsevier: **2016**; Chapter 14, 287-305.
(36) Wanjun, T.; Cunxin, W.; Donghua, C. Kinetic studies on the pyrolysis of chitin and chitosan. *Polym. Degrad. Stab.* **2005,** *87* (3), 389-394.
(37) Corazzari, I.; Nistico, R.; Turci, F.; Faga, M. G.; Franzoso, F.; Tabasso, S. Advanced physico-chemical characterization of chitosan by means of TGA coupled on-line with FTIR and GCMS: Thermal degradation and water adsorption capacity. *Polym. Degrad. Stab.* **2015,** *112*, 1-9.
(38) Zeng, L.; Qin, C.; Wang, L.; Li, W. Volatile compounds formed from the pyrolysis of chitosan. *Carbohydr. Polym.* **2011,** *83* (4), 1553-1557.
(39) Górka, J.; Vix-Guterl, C.; Ghimbeu, C. M. Recent Progress in Design of Biomass-Derived Hard Carbons for Sodium Ion Batteries. *C* **2016,** *2* (4), 24.
(40) Wahid, M.; Gawli, Y.; Puthusseri, D.; Kumar, A.; Shelke, M. V.; Ogale, S. Nutty Carbon: Morphology Replicating Hard Carbon from Walnut Shell for Na Ion Battery Anode. *ACS Omega* **2017,** *2* (7), 3601-3609.
(41) Bommier, C.; Mitlin, D.; Xiulei, J. Internal structure – Na storage mechanisms – Electrochemical performance relations in carbons. *Prog. Mater. Sci.* **2018,** *97*, 170-203.
(42) Qiu, S.; Xiao, L.; Sushko, M. L.; Han, K. S.; Shao, Y.; Yan, M. Manipulating Adsorption–Insertion Mechanisms in Nanostructured Carbon Materials for High-Efficiency Sodium Ion Storage. *Adv. Energy Mater.* **2017,** *7* (17), 1700403.
(43) Raymundo-Piñero, E.; Azaïs, P.; Cacciaguerra, T.; Cazorla-Amorós, D.; Linares-Solano, A.; Béguin, F. KOH and NaOH activation mechanisms of multiwalled carbon nanotubes with different structural organisation. *Carbon* **2005,** *43* (4), 786-795.
(44) Wang, J.; Kaskel, S. KOH activation of carbon-based materials for energy storage. *J. Mater. Chem.* **2012,** *22*, 23710-23725.
(45) Cychosz, K. A.; Guillet-Nicolas, R.; Garcia-Martínez, J.; Thommes, M. Recent advances in the textural characterization of hierarchically structured nanoporous materials. *Chem. Soc. Rev.* **2016,** *46*, 389-414.
(46) Qu, D. Fundamental principals of battery design: Porous electrodes. *AIP Conference Proceedings* **2014,** *1597* (1), 14-25.
(47) Khosravi, M.; Bashirpour, N.; Fatemeh, N. Synthesis of Hard Carbon as Anode Material for Lithium Ion Battery. *Adv. Mat. Res.* **2014,** *829*, 922-926.
(48) Cao, Y.; Xiao, L.; Sushko, M. L.; Wang, W.; Schwenzer, B.; Xiao, J. Sodium Ion Insertion in Hollow Carbon Nanowires for Battery Applications. *Nano Letters* **2012,** *12* (7), 3783-3787.
(49) Bommier, C.; Ji, X. Recent Development on Anodes for Na-Ion Batteries. *Isr. J. Chem.* **2015,** *55* (5), 486-507.
(50) Zhao, C.; Wang, Q.; Lu, Y.; Li, B.; Chen, L.; Hu, Y.-S. High-temperature treatment induced carbon anode with ultrahigh Na storage capacity at low-voltage plateau. *Sci. Bull.* **2018,** *63* (17), 1125-1129.
(51) Wang, S.; Lu (Max), G. Q. Effects of acidic treatments on the pore and surface properties of Ni catalyst supported on activated carbon. *Carbon* **1998,** *36* (3), 283-292.
(52) Board, N. *Gums, Adhesives & Sealants Technology (with Formulae & their Applications) 2nd Edition*, Asia Pacific Business Press: **2010**.

(53) Zhang, B.; Ghimbeu, C. M.; Laberty, C.; Vix-Guterl, C.; Tarascon, J.-M. Correlation Between Microstructure and Na Storage Behavior in Hard Carbon. *Adv. Energy Mater.* **2016,** *6* (1), 1501588.
(54) Hao, R.; Yang, Y.; Wang, H.; Jia, B.; Ma, G.; Yu, D. Direct chitin conversion to N-doped amorphous carbon nanofibers for high-performing full sodium-ion batteries. *Nano Energy* **2018,** *45*, 220-228.
(55) Li, H.; Shen, F.; Luo, W.; Dai, J.; Han, X.; Chen, Y. Carbonized-leaf Membrane with Anisotropic Surfaces for Sodium-ion Battery. *ACS Appl. Mater. Interfaces* **2016,** *8* (3), 2204-2210.
(56) Thrower, P. A. *Chemistry & Physics of Carbon*, CRC Press: Volume 24, **1993**.
(57) Kundu, S.; Xia, W.; Busser, W.; Becker, M.; Schmidt, D. A.; Havenith, M. The formation of nitrogen-containing functional groups on carbon nanotube surfaces: a quantitative XPS and TPD study. *Phys. Chem. Chem. Phys.* **2010,** *12*, 4351-4359.
(58) Frost, R. L.; Hales, M. C.; Martens, W. N. Thermogravimetric analysis of selected group (II) carbonateminerals — Implication for the geosequestration of greenhouse gases. *J. Therm. Anal. Calorim.* **2008,** *95* (3), 999.
(59) Ghimbeu, C. M.; Gadiou, R.; Dentzer, J.; Vidal, L.; Vix-Guterl, C. A TPD-MS study of the adsorption of ethanol/cyclohexane mixture on activated carbons. *Adsorption* **2011,** *17* (1), 227-233.
(60) Ehrburger, P.; Pusset, N.; Dziedzinl, P. Active surface area of microporous carbons. *Carbon* **1992,** *30* (7), 1105-1109.
(61) Ng, S. H.; Vix-Guterl, C.; Bernardo, P.; Tran, N.; Ufheil, J.; Buqa, H. Correlations between surface properties of graphite and the first cycle specific charge loss in lithium-ion batteries. *Carbon* **2009,** *47* (3), 705-712.
(62) Vix-Guterl, C; Couzi, M.; Dentzer, J.; Trinquecoste, M.; Delhaes, P. Surface Characterizations of Carbon Multiwall Nanotubes: Comparison between Surface Active Sites and Raman Spectroscopy. *J. Phys. Chem. B* **2004,** *108* (50), 19361-19367.
(63) Delhaes, P.; Couzi, M.; Trinquecoste, M.; Dentzer, J.; Hamidou, H.; Vix-Guterl, C. A comparison between Raman spectroscopy and surface characterizations of multiwall carbon nanotubes. *Carbon* **2006,** *44* (14), 3005-3013.
(64) Irisarri, E.; Ponrouch, A.; Palacin, M. R. Review—Hard Carbon Negative Electrode Materials for Sodium-Ion Batteries. *J. Electrochem. Soc.* **2015,** *162* (14), A2476-A2482.
(65) Hoekstra, J.; Beale, A. M.; Soulimani, F.; Versluijs-Helder, M.; Geus, J. W.; Jenneskens, L. W. Base Metal Catalyzed Graphitization of Cellulose: A Combined Raman Spectroscopy, Temperature-Dependent X-ray Diffraction and High-Resolution Transmission Electron Microscopy Study. *J. Phys. Chem. C* **2015,** *119* (19), 10653-10661
(66) Olsson, E.; Chai, G.; Dove, M.; Cai, Q. Adsorption and migration of alkali metals (Li, Na, and K) on pristine and defective graphene surfaces. *Nanoscale* **2019,** *11* (12), 5274-5284.
(67) Simone, V.; Boulineau, A.; de Geyer, A.; Rouchon, D.; Simonin, L.; Martinet, S. Hard carbon derived from cellulose as anode for sodium ion batteries: Dependence of electrochemical properties on structure. *J. Energy Chem.* **2016,** *25* (5), 761-768.
(68) Zheng, P.; Liu, T.; Guo, S. Micro-nano structure hard carbon as a high performance anode material for sodium-ion batteries. *Sci. Rep.* **2016,** *6*, Article number: 35620.
(69) Li, Z.; Chen, Y.; Jian, Z.; Jiang, H.; Razink, J. J.; Stickle, W. F. Defective Hard Carbon Anode for Na-Ion Batteries. *Chem. Mater.* **2018,** *30* (14), 4536-4542.

(70) Jiang, Z. Y.; Qu, Z. G.; Zhou, L.; Tao, W. Q. A microscopic investigation of ion and electron transport in lithium-ion battery porous electrodes using the lattice Boltzmann method. *Appl. Energy* **2017,** *194*, 530-539.